Modeling of Sulfation in a Flooded Lead-Acid Battery and Prediction of its Cycle Life

Journal of The Electrochemical Society, 2020 **167** 013538

Modeling of Sulfation in a Flooded Lead-Acid Battery and Prediction of its Cycle Life

K. S. Gandhi[z]

Department of Chemical Engineering, Indian Institute of Science, Bangalore 560012, India

A major cause of failure of a lead acid battery (LAB) is sulfation, i.e. accumulation of lead sulfate in the electrodes over repeated recharging cycles. Charging converts lead sulfate formed during discharge into active materials by reduction of Pb^{2+} ions. If this is controlled by mass transfer of the ions to the electrochemically active area, charging voltage can far exceed the OCV of a charged battery. Then, charge is partly consumed to electrolyse water, and for evolution of hydrogen and oxygen. It causes sulfation since regeneration of active materials will be incomplete. A mathematical model is developed incorporating resistance to mass transfer of Pb^{2+} ions into the rate of charge transfer reactions, changes in areas of active materials and sulfate particles, and dependence of electrodes' resistance on content of lead sulfate. It was used to show that this mechanism of sulfation does lead to failure of flooded LABs because of increased resistance of electrodes, and to predict cycle life. Capacity fade, and increased cycle life when recharging protocol uses lower DoD are other features of degradation which the model predicts. The model also predicts the observed increase in cycle life when conducting additives are added to the negative electrode.

 [DOI: 10.1149/1945-7111/ab679b]

Manuscript submitted September 25, 2019; revised manuscript received December 20, 2019. Published January 15, 2020. *This Paper is part of the JES Focus Issue on Mathematical Modeling of Electrochemical Systems at Multiple Scales in Honor of Richard Alkire.*

List of symbols

a	Active surface area per unit volume, cm^{-1}. Subscripts indicate other areas per unit volume.
C	Acid concentration, mol ml^{-1}. If present, subscripts indicate respective component.
D	Diffusivity of acid in water, $cm^2\ s^{-1}$. Subscripts indicate aqueous diffusivity for other species.
$\mathcal{D}$	Factor reflecting resistance to diffusion
d_c	Critical volume fraction in percolation model.
E°	Equilibrium potential, V
F	Faraday's constant C/(Equivalent weight)
f_o	Initial volume fraction of total solids, $1-\epsilon_o$
I	Applied current density in the cell, A cm^{-2}
i_o	Exchange current density of electrodes, A cm^{-2}. Note they have different values in the positive and the negative. Subscripts indicate the reaction.
$k_{m.s}$	Mass transfer coefficient of sulfate particles, cm s^{-1}.
ℓ	Length scale, cm
L	Thickness of region, cm
M	Molecular weight, g mol^{-1}
n	Number of electrons involved in the reaction = 2.
r	Fraction of active material consumed
$\mathcal{R}$	Gas constant, J $(mol\ K)^{-1}$
S	Rate of charge transfer, A/(cm^3). Subscripts indicate the reaction.
t	Time period. It is time elapsed in the entire test if no subscript is present. s
T	Temperature, K
t^+	Transport number of protons
V	Voltage, V
$\bar{V}$	Molar volume, ml mol^{-1}
x_o	Initial volume fraction of conducting solids in solids, $(\epsilon_{a,o}+\epsilon_{cond,i})/(\epsilon_{a,o}+\epsilon_{cond,i}+\epsilon_{in})$
x	Coordinate along the width of battery, cm

Subscripts

a	Active material
c	Critical value when electrode becomes non-conducting.
ch	In charge phase
$cond, in$	Conducting inerts
$cond, tot$	All conducting solids
dis	In discharge phase
$cell$	Refers to unit cell
eff	Effective value in porous medium
eq	Equilibrium value
g	Gas
in	Non-conducting inerts in electrode
n	Negative
o	Pure or initial state
p	Positive
r	Separator
ref	Reference conditions
s	Lead sulfate, except in ϕ_s

Superscripts

$\circ$	Equilibrium condition

Greek

α	Electrons transferred, subscripts a and c are for anodic and cathodic
δ	Non-dimensional parameter reflecting importance of ohmic losses
$(\Delta V)^*$	$(V_s-V_a)/V_a$
ϵ	Volume fraction of liquid. Subscript refers to volume fraction of solid material indicated by the subscript.
γ	Exponent in percolation theory.
κ	Conductivity of electrolyte, S cm^{-1}
η	Overpotential, V
ϕ	Potential in the electrolyte, V
ϕ_s	Potential in the conducting solid phase of the porous electrode, V
σ	Electronic conductivity of solid, S cm^{-1}
ρ	Density, g cm^{-3}
τ	Time constant, s

Lead–acid batteries (LAB) fail through many mechanisms, and several informative reviews have been published recently as well.[1–5] There are three main modes of failure. (1) As densities of the electrodes' active materials are greater than that of lead sulfate,

[z]E-mail: gandhi@iisc.ac.in

cycles of recharging the battery generate internal stresses leading to formation of cracks in the porous structure. This in turn leads to shedding of active materials from plates. Cracks can also break contact between particles of active materials and loss of electrical continuity. (2) Corrosion of the current collecting lead grids. Grid corrosion leads to debonding between the grid and active materials, and loss of electrical contact. (3) Accumulation of lead sulfate in the electrodes or sulfation. Lead sulfate is sparingly soluble in sulfuric acid, and deposits as particles onto active materials during discharge. These particles dissolve and lead ions are reconverted into active materials in the charging step. During the cyclical recharging operations, if the redissolution-regeneration processes do not fully reverse the effects of precipitation, sulfate accumulates gradually, and active materials are depleted. It will lead to failure because active materials are depleted, and accumulation of sulfate increases the resistance of the battery as well as reduces area for charge transfer reactions. We focus in this article on prediction of failure of flooded lead–acid batteries by sulfation. In passing, we mention that there are other aspects related to the processes of precipitation-redissolution that can accelerate progress to failure. These are Ostwald ripening leading to reduction in area of sulfate particles, and spatially inhomogeneous deposition of sulfate caused when rate of discharge is significantly greater than that of charging.[6] These two will not be considered in this work. We also ignore grid corrosion and fatigue failure, whose effects have to be considered in a complete theory of failure.

Accumulation of sulfate is a result of inadequate supply of charge due to cutoff voltage being reached and or incomplete acceptance of charge toward regeneration. The cell voltage during charging step exceeds the equilibrium voltage of a fully charged battery. If the cell voltage exceeds cutoff voltage before the charge accepted equals the amount discharged, sulfation will be the result. Even when cutoff voltage is not reached, if the cell voltage is sufficiently larger than the OCV of a fully charged battery, electrolytic splitting of water occurs, leading to evolution of hydrogen and oxygen. The latter are referred to as gassing reactions. Gassing reactions consume charge and lead to incomplete utilization of charge toward regeneration of active materials or to sulfation. However, both these occur only when there is a significant rise in the cell voltage during charging, and that is generally attributed to charge transfer being limited by dissolution of lead sulfate. The argument for this goes as follows.

Suppose Q coulombs have been withdrawn in the discharge part of a cycle at some current density. Let us suppose that it is intended to charge the battery at the same rate till Q coulombs have been recharged. Cell voltage decreases during discharge, and it will always be less than that of a fully charged battery. Thus, all Q coulombs withdrawn during discharge of any cycle will go into formation of lead sulfate. However, as charge put in approaches Q, the surface area of lead sulfate particles decreases to a small value. But, lead ions have to dissolve prior to their conversion back into active materials. The charge transfer process is then controlled in part by the rate of dissolution of lead ions from the surface of sulfate particles.[7–9] This additional step adds an extra resistance to charge transfer, and the magnitude of the overpotential will increase. Thus, the charging voltage can be significantly greater than the equilibrium voltage of a fully charged battery, and gassing reactions begin to occur. Then, only a fraction of the charge supplied will go into regeneration of active materials, and sulfate formed during discharge will not be fully reconverted even if Q coulombs are charged. If the rate of dissolution becomes very small, cutoff voltage may be reached even before Q coulombs are charged, and once again, some lead sulfate will remain unconverted. This appears as a plausible explanation for accumulation of sulfate. However, there is a counter point to this argument. The surface area of sulfate particles increases as it accumulates. Hence, at some stage, one might expect the rate of dissolution to not limit conversion of lead sulfate into active materials, and cell voltage may not rise much beyond the OCV of a fully charged battery. Thus, in principle it is possible that, after some cycles of recharging, a cyclical steady state of discharging and charging can be reached. In this work, we resolve this issue by using a mathematical model of the physico-chemical processes occurring in a LAB to calculate the extent of sulfation that can occur over many cycles, and to test if it can lead to failure. The model will thus have the potential to predict the number of cycles after which battery may fail through sulfation. Such a model based on first principles will be more insightful than other available models that utilize neural networks, or electrical circuit analogs, or empirical correlations.

The number of cycles after which a battery fails depends upon the depth of discharge, current density, and the charging protocol. Prediction of the cycle life of a battery, based on the physico-chemical processes occurring, for all types of real time use is at present a distant goal. Instead, one has to settle for prediction of life in a test cycle with the hope that the understanding generated can be put to use to find methods of enhancing cycle life. A simple protocol is used in this work to test the proposed mechanism. Battery is discharged galvanostatically at a current density of about C/5 till a specified DoD is reached. To avoid complications referred[6] to earlier, battery is then charged galvanostatically at the *same* rate till either a cutoff voltage of 2.4 V is reached or all the coulombs discharged are charged back. This recharging protocol is repeated. The latter criteria signalling the end of charging step, perhaps after some initial transients, can keep the battery in a nearly cyclical steady state for long if gassing reactions occur to a very negligible extent. Otherwise, the battery should fail after some number of cycles of recharging. In this work, battery is deemed to have failed when the cell voltage falls below a value of 1.75 V at any instant during the protocol. The cycle life is thus determined if the battery fails. Though the result obtained is specific to the protocol selected, it can be used to predict cycle life with other discharge-charge protocols as the model is based on physico-chemical processes.

There are other known features that accompany degradation of a battery, and the model is tested for its capability to qualitatively predict these as well. It is known that cycle life increases if cycling is carried out between full charge and a decreased DoD. Model is tested against this by employing three values of DoD. The model is also tested for its ability to predict capacity fade. It is also known that addition of carbon to the negative electrode enhances life of a lead-acid battery,[10–14] and several hypotheses have been proposed to account for it. One of them is that addition of carbon improves electrical connectivity though its conductivity is less than that of electrochemically active lead. We propose that addition of conducting inerts increases the percolation threshold of electronic conductivity of the negative electrode, and this can be the mechanism through which such additives enhance life. We put this hypothesis also to test by introducing conducting inerts into the negative electrode and evaluating the cycle life.

Modeling Equations

Firstly, we note that gassing reactions occur only during the charging phase. In flooded designs, unlike in VRLA batteries, a gas-pore network across the separator does not exist for the gases to diffuse through. Thus, hydrogen and oxygen liberated enter the vapor space, and eventually leak out of the battery. Hence, decomposition of hydrogen into hydrogen ions that can occur in the positive electrode, and oxygen recombination that can occur in the negative electrode are not considered here. The main reaction at the positive or lead dioxide electrode is given by

$$PbSO_4(s) + 2H_2O \underset{\text{Discharging}}{\overset{\text{Charging}}{\rightleftharpoons}} PbO_2(s) + H_2SO_4 + 2H^+ + 2e^- \quad [1]$$

The main side reaction that can occur at the positive electrode during charging is evolution of oxygen

$$2H_2O \xrightarrow{\text{Charging}} O_2 + 4H^+ + 4e^- \quad [2]$$

The main reaction in the negative electrode or lead electrode is given by

$$Pb(s) + H_2SO_4 \underset{\text{Charging}}{\overset{\text{Discharging}}{\rightleftharpoons}} PbSO_4(s) + 2H^+ + 2e^- \quad [3]$$

The main side reaction occurring here during charging is the evolution of hydrogen

$$H_2 \xleftarrow[\text{Charging}]{} 2H^+ + 2e^- \quad [4]$$

Mathematical model.—The test cycle does not use very large currents, and hence the effect of capacitance is neglected. A macrohomogeneous model is used. The equations for charge conservation are given by

$$0 = \frac{\partial}{\partial x}\left(\sigma_{eff}\frac{\partial \phi_s}{\partial x}\right) - S \quad [5]$$

where S is the source of charge, and is equal to the rate of flow of charge into the electrolyte per unit volume. In the positive, $S = S_p + S_{oxy}$ while $S = S_n + S_{hyd}$ in the negative. Gassing reactions occur only during charging, and hence S_{oxy} and S_{hyd} are set to zero during the discharge step of the protocol. Charge balance in the fluid phase is given by

$$0 = \frac{\partial}{\partial x}\left(\kappa_{eff}\frac{\partial \phi}{\partial x}\right) - \frac{\mathcal{R}T}{F}\frac{\partial}{\partial x}\left(\kappa_{eff}\frac{1-2t_+}{C}\frac{\partial C}{\partial x}\right) + S \quad [6]$$

The mass balance for acid is given by

$$\frac{\partial}{\partial t}(\epsilon C) = \frac{\partial}{\partial x}\left(D_{eff}\frac{\partial C}{\partial x}\right) - \frac{2t^+ - 3}{2F}S_p - \frac{t^+ - 1}{F}S_{oxy} \quad [7]$$

for the positive electrode and by

$$\frac{\partial}{\partial t}(\epsilon C) = \frac{\partial}{\partial x}\left(D_{eff}\frac{\partial C}{\partial x}\right) - \frac{2t^+ - 1}{2F}S_n - \frac{t^+ - 1}{F}S_{hyd} \quad [8]$$

in the negative electrode. Volume fraction of solids changes only due to the main reactions. Hence, the mass balances for active materials and sulfate are given by

$$\frac{S_p}{2F} = \frac{1}{\bar{V}_a}\frac{\partial \epsilon_a}{\partial t} = -\frac{1}{\bar{V}_s}\frac{\partial \epsilon_s}{\partial t} = \frac{1}{\bar{V}_s - \bar{V}_a}\frac{\partial \epsilon}{\partial t} \quad [9]$$

and

$$\frac{S_n}{2F} = -\frac{1}{\bar{V}_a}\frac{\partial \epsilon_a}{\partial t} = \frac{1}{\bar{V}_s}\frac{\partial \epsilon_s}{\partial t} = \frac{1}{\bar{V}_a - \bar{V}_s}\frac{\partial \epsilon}{\partial t} \quad [10]$$

These equations are fairly standard, and agree with those used by others.[8,9,15,16] The effect of reactions involving water on dilution of acid is ignored here. While the rate of dissolution of lead sulfate particles depends upon their area, charge transfer occurs only on the surface of active materials which can conduct electrons, i.e. only on the active area. The expressions used for evaluation of the active area, the area of sulfate particles, and the rate of charge transfer reactions that include the effects of mass transfer are discussed below.

Area parameters.—As charge transfer occurs, the relative amounts of the active materials and the insulating lead sulfate changes. A commonly used[8,17,18] expression for the area of active materials is

$$a_a = a_o(1 - r)^{1.5} \quad [11]$$

Simple scaling leads to the power of 2/3, but 1.5 is used to account for blocking by lead sulfate particles formed. The above expression is used in this work as well.

Expressions for the rate of the main battery reactions that include effects of mass transfer of lead ions from sulfate particles, as will be seen in the next section, require area of the sulfate particles. A variety of equations have been used[8,9] to calculate this area. Simple scaling would suggest $r^{2/3}$. However, blocking of area would suggest a larger exponent. Here, the following simple expression is used.

$$a_s = a_o r \quad [12]$$

The active area will be different in the two electrodes.

Rate of main charge transfer reactions.—Gassing reactions begin toward the end of the charging period when overpotential increases greatly. Significant rise in the reaction overpotential is needed when the surface area of lead sulfate particles decreases to a low value in order to compensate for the reduction in the overall rate of charge transfer caused by the slow rate of dissolution of lead ions. Expressions that include effect of mass transfer of lead ions on the rate of charge transfer reactions during charging phase have been derived.[6–9] Mass transfer from sulfate particles is not relevant during discharge. The rate expressions are then given by

$$S_{n,dis} = a_a i_o^{ref}\left[e^{\frac{(1-\alpha_c)n\eta F}{\mathcal{R}T}} - e^{-\frac{\alpha_c n\eta F}{\mathcal{R}T}}\right] \quad [13]$$

$$S_{n,ch} = \frac{S_{n,dis}}{\mathcal{D}_n} \quad [14]$$

where

$$\mathcal{D}_n = 1 + \frac{1}{2FC_{s,eq}}\left(\frac{a_a}{a_s}\frac{1}{k_{m,s}}\right)i_o^{ref}\, e^{-\frac{\alpha_c n\eta F}{\mathcal{R}T}} \quad [15]$$

for the lead electrode, and by

$$S_{p,dis} = a_a i_o^{ref}\left(\frac{C}{C_{ref}}\right)\left[e^{\frac{(1-\alpha_c)n\eta F}{\mathcal{R}T}} - e^{-\frac{\alpha_c n\eta F}{\mathcal{R}T}}\right] \quad [16]$$

$$S_{p,ch} = \frac{S_{p,dis}}{\mathcal{D}_p} \quad [17]$$

where

$$\mathcal{D}_p = 1 + \frac{1}{2FC_{s,eq}}\left(\frac{a_a}{a_s}\frac{1}{k_{m,s}}\right)i_o^{ref}\left(\frac{C}{C_{ref}}\right)e^{\frac{(1-\alpha_c)n\eta F}{\mathcal{R}T}} \quad [18]$$

for the positive electrode. The corrections for mass transfer are thus represented by $\mathcal{D}$.

Here, $\eta = \phi_s - \phi - E^\circ$. In the negative, $E^\circ = E^\circ_{Pb}$ the equilibrium potential for Eq. 3, and in the positive, $E^\circ = E^\circ_{PbO_2}$ is the equilibrium potential for Eq. 1. Both are functions of the acid concentration. α_c and exchange current densities will be different in the two electrodes. That rate of charge transfer reaction does not depend on acid concentration in the negative electrode is widely accepted.[9,16,19,20]

Rate of gassing reactions.—Studies on gassing reactions are very few, and have been conducted on VRLA batteries.[8,9,18,20] The reaction overpotentials for both the gassing reactions are large. In view of this, Tafel kinetics have been used by all the investigators for these reactions, and are employed here as well. The rate expression used for Hydrogen evolution is

$$S_{hyd} = -a_a i_{o,hyd}\, e^{\frac{-\alpha_{c,H_2}(\phi_s - \phi)F}{\mathcal{R}T}} \quad [19]$$

where it is assumed that the equilibrium potential of reaction 4 is zero. The rate expression used for Oxygen evolution is

$$S_{oxy} = a_a i_{o,oxy}\, e^{\frac{\alpha_{a,O_2}(\phi_s - \phi - 1.23)F}{\mathcal{R}T}} \quad [20]$$

where 1.23 V is the equilibrium potential with respect to SHE of reaction 2. The equilibrium potentials for *all* the gassing reactions do

depend upon the pH, but for simplicity, all are assumed to be constant.

Electronic conductivity in the electrodes.—Electronic conductivity of the solids of the electrode changes as the relative contents of active materials and lead sulfate are altered by the charging and discharging processes. Percolation model is used to account for this. Percolation model proposes that conductivity of a mixture of particles scales as

$$\sigma \sim (\epsilon_{cond,tot} - d_c)^{\gamma} \quad [21]$$

Expression for effective conductivity based on percolation theory reported earlier[21,22] is used here as well.

As mentioned in the introduction, it is proposed to examine if addition of inert but conducting materials to the negative electrode will extend cycle life. This needs a theory for predicting conductivity of mixtures of particles of four kinds of solids: conducting active materials, insulating sulfate particles, inert but insulating materials, and inert but conducting materials. Expressions presented earlier account for presence of only insulating and conducting particles. However, these expressions can account for the presence of the first three kinds of particles since insulating sulfate and inert but insulating particles can be lumped into a single type of material. However, particles with different conductivities cannot be lumped together. The percolation threshold, i.e. the critical volume fraction d_c of conducting solids, which must be exceeded for the mixture to be conducting is independent of conductivities of individual components in a multicomponent mixture according to percolation models. However, percolation models for predicting effective conductivity of mixtures of conducting particles with different conductivities when their total volume fraction is above d_c are not available. Effective medium theories are an alternative, but are not satisfactory for predicting the sharp transition in conductivity near the percolation threshold. Hence, a compromise has to be adopted. Thus, in order to test the effect of addition of conducting but inert materials, a simplification is made here. Emphasizing the behavior near the percolation threshold, it is assumed here that the conductivity of the active material and inert but conducting material are equal. The simplification allows us to treat the mixture of particles as consisting of only two kinds of solids. The expression for conductivity is now given by

$$\sigma_{eff} = \sigma_o(1 - \epsilon - \epsilon_{in})^{0.5} \times \left[\frac{\frac{\epsilon_{cond,in}}{f_o} r + x_o(1 - r) - \frac{d_c}{f_o}}{\left(1 + (x_o - \frac{\epsilon_{cond,in}}{f_o})(\Delta V)^* r\right)\left(x_o - \frac{d_c}{f_o}\right)} \right]^{1.7} \quad [22]$$

r is the fraction of active material reacted and is given by

$$r = 1 - \frac{\epsilon_a}{\epsilon_{a,o}} = 1 - \frac{\epsilon_a}{1 - \epsilon_o - \epsilon_{cond,in} - \epsilon_{in}} \quad [23]$$

Conductivity goes to zero when fractional conversion reaches a critical value such that the volume fraction of all the conducting solids is given by $\epsilon_{cond,in} + \epsilon_{a,o}(1-r_c) = \epsilon_{cond,in} r_c + f_o x_o (1 - r_c) = d_c$. Equation 22 reduces to the earlier expressions[21,22] when the volume fraction of conducting inerts is zero.

Percolation model thus can be used to calculate the effective conductivity of the electrode as a function of the sulfate content, or the fractional conversion of active materials, r. The conductivity goes to zero when the fractional conversion equals r_c, and this value is referred to as the critical conversion. When the electronic conductivity of a part of an electrode goes to zero, current cannot pass through that part. Thus an important consequence of this is that charge transfer reactions cannot occur on that part of the electrode.

Boundary and initial conditions.—Figure 1 shows a cell of a lead–acid battery that is customarily used in modeling. It consists of

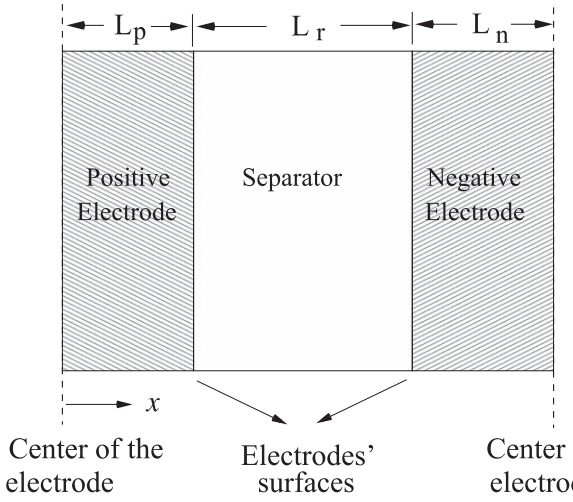

Figure 1. Schematic of a unit cell of lead acid battery used in the model.

electrodes of half their thicknesses with a separator saturated with acid. Standard boundary conditions are used. For the solid phase of the electrode, current density as prescribed by Ohm's law is used at $x = 0$, while current density at $x = L_p$ and $x = L_p + L_r$ is set to zero. Zero current density and zero mass flux of acid are employed at $x = 0$ and $x = L_p + L_r + L_n$ in the fluid phase. Continuity of potential, current density, concentration, and mass flux of acid are used at all the other interfaces for the fluid phase. One value of the potential can be arbitrarily set and $\phi_s = E^o_{Pb}(C_{ref})$ at $x = L_p + L_r + L_n$ was used. These are standard conditions used, and corresponding equations are not repeated here as they are same as given earlier.[16,23] Initial condition for discharge in the first cycle was a cell with uniform concentration of acid and zero sulfate content every where.

Results and Discussion

Model parameters & methodology.—Dimensions of the battery used are given Table I, and these are same as those used earlier.[23,24] The only difference is that volume fraction of inerts in the positive was reduced slightly to make the negative active material to be the limiting reactant. Values for all the other parameters appearing in the model equations except for the gassing reactions are same as those used earlier[23] and are also given Table I for ready reference.

Data on flooded batteries with all attendant details about gassing reactions could not be found in published literature. As mentioned earlier, studies on gassing reactions are few,[8,9,18,20] and were conducted on VRLA batteries. Evaluation of parameters from data obtained in those studies focused on end stages of charging where pressure is observed to increase and voltage shows a peak. Values for the kinetic parameters used by them are listed in Table II. As can be seen from Table II, the cathodic transfer coefficient is generally accepted to be 0.5 for hydrogen evolution. It can be seen from Table II that values of exchange current densities reported for hydrogen evolution reaction are very different. It may be kept in mind that hydrogen evolution is not significant till the very end stages in VRLA batteries since oxygen recombination is the dominant reaction. A value of 1.0×10^{-12} A cm^{-2} was used for $i_{o,hyd}$ in this work. The anodic transfer coefficient is generally accepted to be 2 for oxygen evolution. Values of exchange current density of the oxygen evolution reaction also vary widely between the above cited authors. Here, the values are perhaps fitted to adjust for the recombination rates of oxygen that occurs in VRLA batteries. A value of 1.0×10^{-37} A cm^{-2} was chosen in this work.

The other important parameter is the mass transfer coefficient of dissolution of lead ions from the surface of lead sulfate particles. However, rate of mass transfer during dissolution of sulfate has received little attention in the literature. As the particle size becomes very small, the mass transfer coefficient should increase, but it is

Table I. List of model parameters.

Symbol	Name	Unit	Positive	Reservoir	Negative
L	Region thickness	cm	0.1095	0.33	0.0915
ϵ_o	Porosity		0.52	1.0	0.61
ϵ_{in}	Volume fraction of inerts		0.08	0.0	0.057
	When conducting inerts are present		0.08	0.0	0.032
$\epsilon_{cond,in}$	When conducting inerts are present		0.0	0.0	0.025
a_o	Maximum active surface area	cm^{-1}	2.3×10^5		2.3×10^4
i_o^{ref}	Reference exchange current density.	A cm^{-2}	9.0×10^{-7}		9.0×10^{-6}
$2(1-\alpha_c)$	Anodic transfer coefficient		1.15		1.55
$i_{o,hyd}$	Exchange current density for hydrogen evolution.	A cm^{-2}			1.0×10^{-12}
α_{c,H_2}	Cathodic electrons				0.5
$i_{o,ox}$	Exchange current density for Oxygen evolution.	A cm^{-2}	1.0×10^{-37}		
α_{a,O_2}	Anodic electrons		2.0		
σ_o	Electrical conductivity	S cm^{-1}	80		4.8×10^4
d_c	Packing parameter		0.154		0.154
$k_{m,s}$	Mass transfer coefficient	cm s^{-1}	0.05		0.05
$\bar{V}_a$	Molar volume	mol ml^{-1}	24.659		18.271
Parameters applicable to entire cell					
C_{ref}	Initial and reference concentration		mol ml^{-1}	4.97×10^{-3}	
I_{cell}	Current density for discharge		A cm^{-2}	−0.078 2	
I_{cell}	Current density for charge		A cm^{-2}	0.078 2	
$\bar{V}_s$	Molar volume of $PbSO_4$		mol ml^{-1}	48.139	
T	Temperature		K	298.15	
t^+	Transport number			0.72	

Table II. Exchange current densities of gassing reactions on lead electrode.

Hydrogen evolution on lead electrode		Oxygen evolution on lead dioxide electrode		Reference
$i_{o,hyd}$, A cm^{-2}	α_{c,H_2}	$i_{o,oxy}$, A cm^{-2}	α_{a,O_2}	Reference
4.79×10^{-12}	0.476			Bockris and Srinivasan[25]
		3.5×10^{-39}	2	Bernardi and Carpenter[18]
2.4×10^{-11}	0.5	3.7×10^{-41}	2	Newman and Tiedemann[8]
1.6×10^{-12}	0.5	1.9×10^{-41}	2	Srinivasan et al.[20]
5×10^{-14}	0.5	3×10^{-28}	2	Cugnet et al.[16]
2.5×10^{-9}	0.473	5×10^{-20}	0.61	Bernardi et al.[9]

very likely that dissolution is then limited by rates of incorporation of ions into the lattice. Hence, a constant mass transfer coefficient is used in literature. Once again, values provided by different investigators[7–9,26] vary widely, ranging from 10^{-4} to 10^{-2} cm s^{-1}. A value of 0.05 cm s^{-1} is used here.

The battery selected for simulation[23,24] has a nominal capacity of 30 Ah at C/5 rate. Galvanostatic discharge was carried out at a current density of −0.007 82 A cm^{-2}, and it corresponds to C/5 rate for this battery. 30 Ah also corresponds to 140.7 C cm^{-2}. This figure was used to define depth of discharge. Three values of coulombs drawn were used: 130 C cm^{-2}, 117 C cm^{-2}, and 105 C cm^{-2}. These correspond to DoD of 92.4%, 83.22%, and 74.6% respectively. Charging was done at the same current density so that effects of asymmetry between discharging and charging were eliminated, and focus will be on sulfation in the most simple scenario. Galvanostatic charging was done till either a voltage of 2.4 V is reached or till the coulombs drawn were charged. Rest period was not used.

Details of the numerical method used to solve the model equations, and parametrized expressions for $E^\circ(C)$, D_{eff}, and κ_{eff} are the same as used earlier.[23] Solubility of lead sulfate at C_{ref} was used for $C_{s,eq}$. Numerical solution was deemed to be converged when successive iterates of all non-dimensional variables differed by not more than 10^{-6}. Electrical conductivity of electrode was equated to a very small value of 10^{-8} S m^{-1} when critical conversion was reached instead of setting it to zero to prevent numerical divergences.

Cycle life of the battery without conducting inerts.—We begin by showing our main result that the battery without addition of conducting inerts does fail due to sulfation, and thus cycle life could be predicted. The DoD employed for the simulation was 92.4%, i.e. 130 C cm^{-2} were to be discharged. The cutoff voltage of 1.75 V will be reached only during discharge step since cell voltage will be greater than the equilibrium voltage during charging step. Figure 2 shows the voltage at the end of discharge step in each cycle. It can be seen that the cutoff voltage is reached in the 104th cycle. Polarization curve for the 104th cycle displayed in Fig. 3 shows that the battery failed before 130 C could be discharged. Thus, cycle life for the battery is 103 cycles. It also can be seen from Fig. 2 that voltage at the end of discharge hardly changes for many cycles, and it drops steeply only toward the end of its life. This aspect is reinforced by the temporal profile of cell voltage during discharge shown in Fig. 3 for a few cycles. The curves display typical polarization behavior. It can be seen that voltage drops significantly only after 100 cycles. The predicted cycle life is clearly dependent upon the choice of parameters, especially the exchange current densities for the gassing reactions. If the gassing reactions occur faster, the cycle life will be shorter. As the negative electrode is only marginally less in stoichiometric capacity compared to that of the positive electrode, the value chosen for oxygen evolution reaction also affects the cycle life predicted in this work. Clearly, considerable data are needed to accurately fix the values for these two parameters. It can also be seen from Fig. 2 that there are

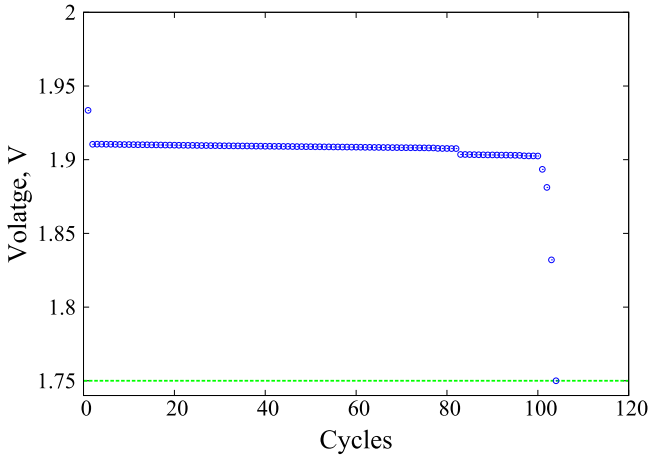

Figure 2. Cell voltage at the end of discharge for all the cycles for a battery which does not contain conducting inerts. It is plotted against cycle number. The horizontal line at the bottom corresponds to 1.75 V.

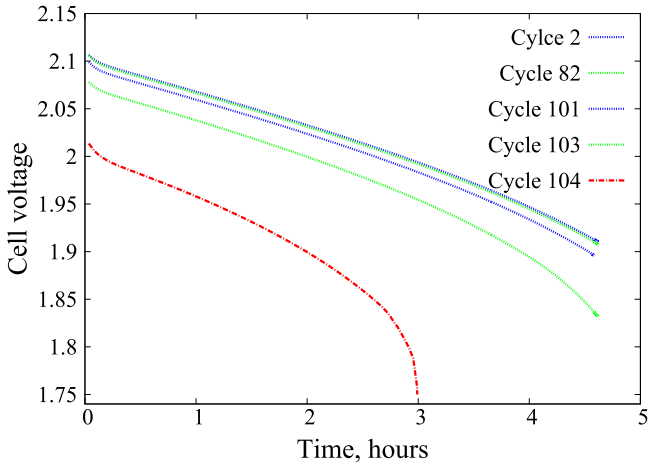

Figure 3. Cell voltage as a function of time elapsed during the discharge step is shown for a few cycles.

discontinuous jumps at the end of cycles 82, 101, 102, 103, and 104. It may be noted that every cycle brings a finite change in the cell voltage, and only the changes much larger in magnitude are referred to as discontinuities. Discontinuities cannot be attributed to time step and grid size chosen since the customary tests for insensitivity to both these have been carried out for all the other results. The discontinuities arise out of discretization of the electrodes into small finite volumes for the purposes of numerical solution. Only gradual changes will be observed, and this point will be discussed a little later.

Data on cell voltage at the end of all charging steps are presented in Fig. 4. It can be seen from the inset of Fig. 4 that charging stops when cell voltage reaches 2.4 V only for the first two cycles. Thus, as per the recharging protocol, the entire charge of 130 C withdrawn during the preceding discharging step could not be charged in the first two cycles. As a result, some amount of sulfate did accumulate during these two cycles. After the first two cycles however, cell voltage at the end of charging step remains below 2.4 V, and monotonically decreases, till 82nd cycle. Hence, as dictated by the charging protocol, beginning from 2nd cycle till 82nd cycle, all of 130 C withdrawn during the preceding discharge step have been accepted during the charging step. However, it does not entirely go into regenerating active material, and sulfate content does increase. This can be seen from Fig. 5 where spatial distribution of volume fraction of sulfate for a number of cycles of recharging is shown for both the positive and negative electrodes. Figure 5 shows a

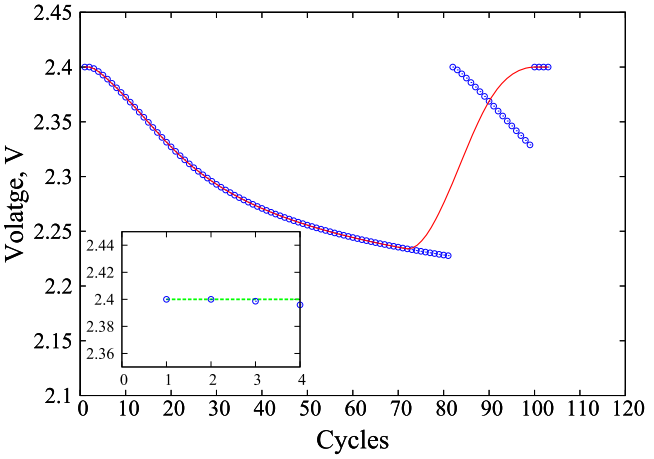

Figure 4. Cell voltage at the end of charging step for all the cycles for a battery which does not contain conducting inerts. It is plotted against cycle number. Inset shows the same data for the first four cycles. Continuous line shows what would be observed.

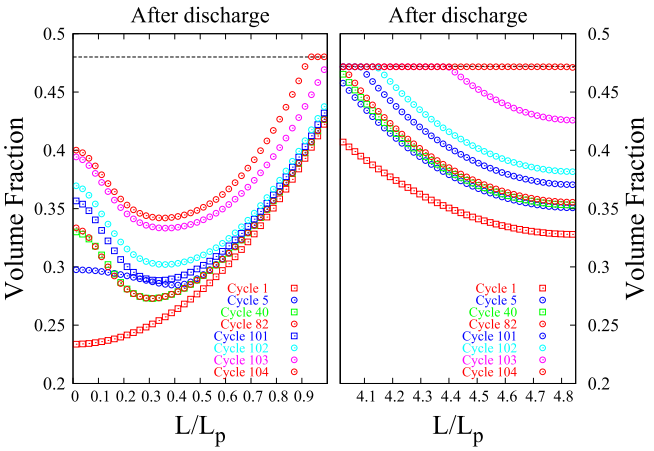

Figure 5. Volume fraction of lead sulfate as a function of position in the battery at the end of discharge for different cycles. Results for the positive and negative are shown in the left and right panels respectively. Volume fraction at critical conversion is shown by dotted line at the top. The curves are in the order presented, and can be identified easily by looking at the right side of the two panels.

monotonic increase in the overall sulfate content in both the electrodes with increasing number of cycles of recharging. Thus, the cell voltage at the end of charging step, though below 2.4 V, is high enough for gassing reactions to occur and hence lead sulfate continues to accumulate with increasing cycles of recharge.

One consequence of sulfate accumulation is a decrease in the electronic conductivity, though the rate of decrease will be slow till percolation threshold is approached. Increase in electrical resistance would suggest that the cell voltage at the end of charging step must not fall below 2.4 V. However, increase in sulfate content also means increased area of sulfate particles. This reduces resistance to mass transfer, and lowers surface overpotential. Effect of this is a reduction in cell voltage needed to charge, exactly opposite to what increased resistance does. The effect of increased surface area dominates the effect of slowly increasing resistance, and cell voltage at the end of charging step steadily decreases from 2.4 V with increasing cycles of recharging. This trend however is disrupted as the critical conversion is approached when the electronic conductivity sharply tends to zero at some location in the electrode. This has important consequences and will be discussed below.

In both the electrodes, the dimensionless ratio[27] of loss of potential due to ohmic resistance to that due to charge transfer

reaction at the surface is of the order of unity. Similarly, the ratios[27] of electrode thickness to penetration depth due to diffusion are also of the order of unity. The values for these ratios indicate some inhomogeneity in the utilization of the electrode, it being more pronounced in the positive than in the negative. As a result, reaction proceeds to a greater extent near the electrode-electrolyte interface than in the interior. This is confirmed by the trends in Fig. 5 where sulfate content is seen to decrease toward the center of the electrode. Let us examine in detail results for the negative electrode first. It can be seen from Fig. 5 that, after a few initial cycles of transient nature, the volume fraction in the negative appears to be reaching a quasi-steady profile till about 80 cycles. Due to the steady increase in sulfate content however, critical conversion is attained at the end of discharging step of the 82nd cycle at the first grid point near the separator-electrode interface. When electronic conductivity falls to zero at any grid point, current cannot pass through the finite volume corresponding to that grid point. Hence, charge transfer reactions cannot occur, and charge can neither be withdrawn from nor supplied to that finite volume. Hence, from the time when the conductivity falls to zero till the battery fails, the finite volume associated with *any* grid point that turned insulating will remain electrochemically inactive. As a result, porosity, volume fraction of active materials, and volume fraction of sulfate will remain unchanged in any finite volume that is electronically non-conducting. However, ions can still pass through the electrolyte, and charge transfer reactions can occur at other grid points whose conductivity is not zero. The battery will therefore function till a large enough fraction of electrode turns insulating and the cutoff voltage of 1.75 V is reached.

As the first finite volume in the negative electrode has become electrochemically inactive during the 82nd cycle, the cell voltage at the end of charging step jumps to 2.4 V as seen from Fig. 4, and less than 130 C would have been charged in this cycle leading to a sudden increase in the accumulation of lead sulfate. Correspondingly, a discontinuous change in cell voltage is also observed in Fig. 2. This pattern continues whereby cell voltage at the end of charging gradually decreases from 2.4 V, and jumps back to 2.4 V when more grid points turn insulating. The next discontinuity occurs at the end of discharging step of the 101st cycle. At the end of discharge of this cycle, as many as three grid points out of a total of forty turned insulating. As a result, much less than 130 C could be charged during charging step of this cycle. Accumulation of sulfate thus accelerates with each subsequent cycle. Cell voltage at the end of charging steps attains 2.4 V during 101st, 102nd, and 103rd cycles, and less than 130 C would have been accepted during charging step of all these cycles. As a result, more grid points turn insulating, and greater fraction of the electrode turns inactive. This is reflected in the discontinuous changes in the cell voltage seen in Figs. 2 and 4. The discontinuities seen in Fig. 2 occur at the end of 102nd, and 103rd cycles when six, and eighteen grid points turn insulating, respectively. As many as thirty four grid points turned insulating during discharging step of the 104th cycle, though most of the grid points excepting the last one were close to critical conversion. As a result, cell voltage during the discharging step reached 1.75 V before the expected discharge of 130 C could be completed. Thus, battery is deemed to have failed during the 104th cycle.

Now, we will return to the point about discretization and discontinuities. As discharge proceeds, the electrode gets divided into two zones once critical conversion is reached at the electrode-electrolyte interface. One zone is a conductor while the other is an insulator. The entire battery can consist of five zones: the separator, and two each in the electrodes. While the boundaries of the separator are fixed, the boundaries between the two zones in both the electrodes move with time, and the thicknesses of the insulating zones increase with time. This constitutes a complex moving boundary value problem, and solving it exactly is numerically expensive. As an alternative, in the calculation carried out here, each electrode was divided into 40 discretized finite volumes. Thus,

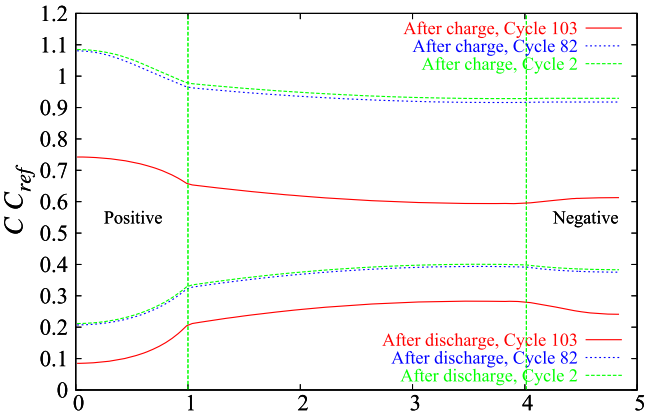

Figure 6. Spatial profile of acid concentration at the end of 2nd, 82nd and 103th cycles. The top three curves are for charging step while the bottom three are for the discharge step.

while the boundary between the two zones in an electrode moves across a finite volume steadily, in the discretized calculation, it jumps from the beginning of the finite volume to its end when the electronic conductivity at the grid point located in the middle of the finite volume becomes zero. For example, while the boundary steadily traverses through the second finite volume between 83nd and 101st cycles, it will appear as a jump across the finite volume during the 101st cycle. The gradual increase in the insulating fraction of the finite volume is compensated for all at once. The calculated discontinuities in the cell voltage are a consequence of this. Observations however will show only a gradual variation. The observations can be expected to be close to a smooth curve drawn using the midpoints between discontinuities, and is shown in Fig. 4. Behavior of the first finite volume, i.e. next to the electrode-electrolyte interface, is slightly different. The insulating zone does not begin to form till conductivity falls to zero at the electrode-electrolyte interface. In order to draw the smooth curve, the cycle during which insulating zone *begins* to form in the first finite volume was taken to be that in which nondimensional conductivity falls to 0.5, i.e. utilizing the usually assumed linear variation across a finite volume. The projected smoothed results must be taken to be approximate. Suppose the number of grid points, and hence the number of finite volumes, were to be increased. The number of discontinuities will increase. Referring to Fig. 2, there will be more discontinuities between 83nd and 101st cycles, and it may not take the same number of cycles to reach the same state of electrode as it was at the end of the 101st cycle. Similarly, while 50% of the electrode was inactive at the end of 101st cycle, and it grew to 90% during the 104th cycle, enhanced number of grid points is likely to change the number of cycles over which this happens. Thus, the results presented should be treated conservatively, and the number of cycles needed to reach failure may be less than predicted.

Let us turn our attention to the positive electrode. In Fig. 5, a minimum in the volume fraction of sulfate is seen in the positive while it is absent in the negative. This indicates that charging step near the center of the positive electrode is less effective in regenerating active material. This can be understood as follows. In the positive, the inhomogeneity is greater, and rate of the charge transfer reaction that regenerates active material is proportional to the acid concentration. Inhomogeneity is greater since the σ of the positive is two orders of magnitude smaller, and the thickness of the positive electrode is 20% greater. Very importantly, the latter also increases the resistance to diffusion of acid. While the portions of the electrode near the separator are unaffected by this, the diffusive flux of acid into the interior of the positive electrode is reduced, and its concentration there is reduced. (See Fig. 6). Hence, rate of the reaction that regenerates active material decreases in the interior of the positive. It may be mentioned that the decrease in acid concentration can increase the rate as overpotential increases, but

Table III. Variation in cycle life with depth of discharge.

Coulombs discharged	Cycle life
130, 92.4%	103
117, 83.2%	876
105, 74.6%	1854

this effect is much weaker. More over, the rate of the charge consuming oxygen evolution reaction, which occurs only during the charging step, is independent of acid concentration. Thus, regeneration of active materials during charging is less than the generation of sulfate during the discharge step in the interior of the electrode. As a result, a minimum is seen in the profile of sulfate in the positive. The profiles move up almost in a parallel manner after 82nd cycle when the functioning of the battery is determined by the ever increasing fraction of negative which becomes non-conducting. The area of sulfate particles is greater in this electrode than in the negative electrode, and hence effect of mass transfer resistance is also less significant. Further, in comparison with the negative electrode, relative to the main battery reaction, the side reaction generating oxygen is more slow. Both these effects lead to a slower accumulation of sulfate in this electrode than in the negative. The critical conversion leading to percolation threshold is also larger in this electrode than in the negative electrode since the positive has a slight stoichiometric excess of active material than the negative. Due to all these factors, even though several grid points turn insulating in the negative electrode, the entire positive electrode remains active till the end of the 103rd cycle. In the positive electrode, significant accumulation of sulfate occurs during 102nd and 103rd cycles where less than 130 C were accepted during charging step of all these cycles. Even then, during the discharging step of the last 104th cycle only three grid points turn insulating. Failure of the battery thus cannot be attributed to the positive.

Decrease in cell voltage at the end of discharging step, as well as increase in cell voltage needed to charge, are also caused by another factor. Incomplete conversion of lead sulfate is also accompanied by incomplete regeneration of acid, and this has not been stressed enough so far. This is important since the equilibrium voltage of the cell is sensitively dependent on concentration of sulfuric acid, and it decreases as concentration of acid decreases. This contributes significantly to lowering of the cell voltage during discharge as acid is not regenerated. The acid concentration profiles for the second cycle, 82nd cycle, and 103th cycle are shown in Fig. 6. As discussed earlier, full charge of 130 C was accepted in the charging step after the first two cycles. Thus, after an initial transient, the concentration profile does not change much from 2nd to 82nd cycle. After that, especially after 101st cycle, as more and more grid points turn insulating, less and less charge is accepted during the charging step. Due to this, just as volume fraction of sulfate increases as seen from Fig. 5, acid concentration also decreases. This decrease has a significant effect. Thus, while $E^{\circ}_{PbO_2}$ and E°_{Pb} are equal to 1.72 V and -0.37 V respectively at acid concentration of 5 mol liter^{-1}, these reduce to 1.62 V and -0.286 V respectively, at a concentration of 0.75 mol lit^{-1}. This contributes significantly to the lowering of the cell voltage to 1.75 V, the value at which battery is deemed to have failed.

Effect of depth of discharge on cycle life.—The effect of depth of discharge on cycle life was studied by lowering the depth of discharge by changing the coulombs withdrawn to 117 C and 105 C in place of 130 C used in the previous section. It is expected that the cycle life should increase when a battery is cycled to a lower depth of discharge. Table III shows that cycle life did increase along the expected lines. Other features such as spatial profiles of volume fraction of lead sulfate, and acid concentration in the two electrodes etc. are similar to those seen earlier, and are thus not shown. In particular,the model predicts that the fraction of the negative electrode that attains critical conversion, and hence becomes inactive, is nearly the same. When the depth of discharge is decreased, the extent of conversion of active materials during discharge in any cycle decreases. As charging is done to the same capping voltage of 2.4, the accumulation of sulfate per cycle is approximately the same. However, the model predicts that for the battery to fail, the fraction of the electrode that should attain critical conversion nearly the same. Thus, starting from a smaller conversion due to decreased depth of discharge, more cycles are required for the critical conversion to be attained. As a result cycle life increases with a decreased depth of discharge.

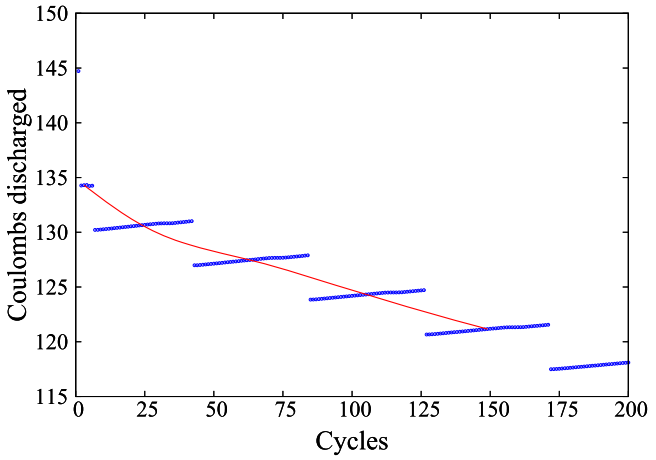

Figure 7. Capacity of a battery during discharge is shown against the number of cycles of recharge. The smooth line is drawn as explained in the text.

Cycle life at 74.6% depth of discharge appears to be quite large. Thus, one would guess that the cycle life of a battery is determined not just by sulfation. There are several other degradation mechanisms. Thus grid corrosion, and fatigue failure will lead to shedding and electrical isolation. Positive plate can fail due to changes in $\alpha/\beta - PbO_2$ ratio. During the course of cycling, the positive active mass can lose its intrinsic activity described by the hydrogen-loss model. The cycle life would be the minimum predicted by any of these three mechanisms assuming that these operate independently. Two models of grid corrosion have been published.[28,29] Kim et al.[29] use an empirical expression for the growth of a film formed due to corrosion, but do not consider sulfation at all. Boovaragavan et al.[28] do treat corrosion reaction as an electrochemical reaction, but they also do not consider sulfation. They do not present any comparison with data. The parameters in these models need to be fitted to some independent measurements of the effects of grid corrosion before they can be used along with the model of sulfation.

Capacity fade.—Another known feature of degradation is the decrease in the capacity of a battery during discharge step with increasing number of cycles of recharge. Here, discharge up to 1.9 V followed by charging up to a capping voltage of 2.4 V was the recharging cycle chosen. A plot of the coulombs that could be discharged in successive cycles against cycle number is shown in Fig. 7. Calculations were carried out up to 200 cycles, and the results conform to the expected trend. The first cycle is a transient and shows the highest capacity, and the capacity falls steeply in the next cycle itself. There after, the capacity fade is gradual. The discontinuities in the plot occur for the same reasons discussed earlier, and the smooth curve is drawn as explained earlier. Once again, all the other features such as spatial profiles of volume fraction of lead sulfate etc. are similar to those found earlier, and are thus not shown. As pointed during discussion of discontinuities, the results must be treated conservatively, and the capacity fade could occur faster than predicted.

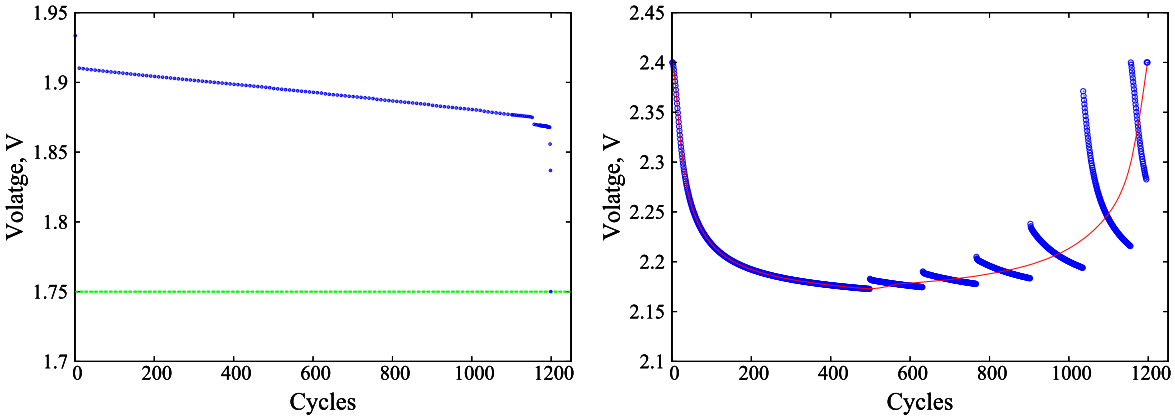

Figure 8. Left panel shows cell voltage at the end of discharge for all the cycles for a battery to which conducting inerts have been added to a volume fraction of 0.025. It is plotted against cycle number. Green horizontal line is at 1.75 V. Right panel shows cell voltage at the end of charge for all the cycles for a battery to which conducting inerts have been added to a volume fraction of 0.025. It is plotted against cycle number.

Effect of addition of conducting inerts on cycle life.—At the outset, it must be pointed out that addition of carbon to the negative electrode has many effects, and one of them can even be enhancement of hydrogen evolution reaction.[14] Thus, this section has to be treated as an effort to elicit the effect of adding conductive *inerts*, which do not have any other effects such as enhancing hydrogen evolution reaction, increasing active area for the main battery reactions etc.. Conducting inerts were added only to the negative electrode. As indicated in Table I, the total volume fraction of the inerts was kept constant at 0.057 in order to avoid any extraneous variations. Volume fraction of the conducting inerts was set at 0.025. As mentioned earlier, Eq. 22 was derived assuming that conductivities of the active material and conducting inerts are equal. Here, the conductivity of conducting inert was assumed to be equal to that of lead.

The recharging protocol is the same as used, and 130 C were discharged (DoD of 92.4%). Left panel of Fig. 8 shows the cell voltage at the end of discharge step as a function of cycle number. The battery fails during the discharge step of the 1199th cycle, and the battery life is now equal to 1198 cycles. Addition of inert but conductive additive has greatly extended cycle life. The extent of the increase is obviously dependent on the assumption of equating the conductivities of active and inert materials. The features in this Fig. are similar to those observed in Fig. 2. The critical conversion of the active materials in the negative can be calculated from Eq. 22. In the case under consideration where conducting additives are added, it is equal to 0.6126, while it was equal to 0.5375 in the absence of conducting inerts. The battery thus functions till a higher conversion of active materials is reached, and that is the main reason for the increase in the life of the battery. As the critical conversion is larger than when conducting inerts are absent, more cycles are now needed for the same fraction of electrode to turn insulating. Further, area of sulfate particles is also now more since they are present to a greater volume fraction. Hence, the entire process accumulation of sulfate is slowed down due to the reduced mass transfer resistance. When conducting inerts were added, one grid point turned insulating during the discharge step of cycle numbers 500th, 633rd, 767th, 903rd, 1036th, and 1156th. Thus, there is a slow but regular increase in the inactive fraction of the electrode. By the end of the discharge step of 1156th cycle, a significant fraction of the electrode has turned insulating and process of decay speeds up from then on. The next grid points turns insulating during the discharge steps of 1192rd cycle, and 1196th cycle. Battery fails during the discharging step of 1199th cycle when 20 grid points turned insulating. Battery has failed here even when less number of grid points turned insulating compared to the case when conducting inerts are absent for the following reasons. The volume fraction of sulfate at critical conversion is now equal to 0.5375 while it was 0.4716 when conducting inerts were absent. The volume fraction of solids in all the grid points is now greater, and hence the effective ionic conductivity and diffusivity of acid are reduced considerably. It contributes to increased losses in potential. Data on cell voltage at the end of charging cycles are shown in the right panel of Fig. 8. The characteristics seen in the Fig. are similar to those found in Fig. 4, and the former is a slowed down version of the latter. The spatial profiles of volume fraction of lead sulfate in both the electrodes, and spatial profiles of acid concentration in the two electrodes are similar to those shown for the case where conducting inerts have not been added. They are thus not shown.

Some inferences.—It was shown that sulation occurs due to gassing reactions, which consume charge and prevent complete regeneration of active materials. Sulfation reduces the life of a battery. Hence, reducing the rate of gassing reactions can enhance cycle life. Reducing cutoff voltage for charging is one such way. Reducing the depth of discharge is another way to improve cycle life. Both these methods would decrease the charge available for utilization per cycle. Addition of conducting inerts is another way to enhance cycle life. Another possibility is to reduce the resistance to mass transfer during the charging step. This can be achieved if the area of sulfate particles can be increased. This would be possible, assuming the same extent of nucleation per unit area, by increasing the surface area of the negative electrode. Increasing overvoltages for hydrogen and oxygen evolution reactions is another way of reducing gassing reactions. Occurrence of gassing reactions is related to the high levels of charging voltage, and is independent of which of the active materials of the battery are the limiting reactants. Hence, we can expect the results to be relevant even if acid is the limiting reactant, e.g. in VRLA batteries.

Conclusions

Accumulation of lead sulfate, or sulfation, is one of the causes of failure of a flooded lead-acid battery. As complete conversion of lead sulfate into active material is approached during the charging step, resistance to mass transfer of lead ions to active area becomes significant, and overpotential increases to such an extent that charge consuming hydrogen and oxygen evolution reactions due to water splitting begin to occur to a significant extent. This leads to incomplete conversion lead sulfate of to active materials, and its accumulation over repeated recharging cycles. One objective of this work was to test if this mechanism explains sulfation. When volume fraction of lead sulfate in any part of the electrode attains a critical level dictated by percolation theory, that portion of the electrode turns electronically insulating, and hence electrochemically inactive. As lead sulfate accumulates in the electrode over repeated cycles of

recharge, inactive zones form in the electrode, and their thickness continually increases. Consequently, at some point during discharge, the battery can fail as cell voltage falls below a prescribed value, usually taken to be 1.75 V. Another objective of this work was to check if the extent of sulfation proceeds to such an extent to lead to failure. A mathematical model that incorporates the relavant physico-chemical processes was developed. The model was used to demonstrate that sulfation occurs due to charge consuming gas evolution reactions, and it leads to failure of the battery. The model could make quantitative predictions of the cycle life, effects of DoD on cycle life, and capacity fade. It was also shown that addition of conducting inerts enhances the cycle life by increasing the critical volume fraction of lead sulfate where the conductivity falls to zero. Several suggestions to increase the cycle life were made based on the role played by gassing reactions in the degradation of a battery.

Acknowledgments

Author thanks Prof. Raj Pala of IIT Kanpur for his valuable critique of the manuscript.

References

1. H. A. Catherino, F. F. Feres, and F. Trinidad, *J. Power Sou.*, **129**, 113 (2004).
2. P. Ruetschi, *J. Power Sou.*, **127**, 33 (2004).
3. D. U. Sauer, "Secondary batteries: lead acid batteries—life determining processes." in *Encyc. of Electrochem. Power Sou.*, ed. J. Garche (Elsevier, Amsterdam) Vol. 4, p. 805 (2005).
4. Y. Guo, S. Tanga, G. Meng, and S. Yang, *J. Power Sou.*, **191**, 127 (2009).
5. M. R. Palacín and A. de Guibert, *Science*, **351**, 1 (2016).
6. K. S. Gandhi, *J. Electrochem. Soc.*, **164**, E3092 (2017).
7. D. Simonsson, P. Ekdunge, and M. Lindgren, *J. Electrochem. Soc.*, **135**, 1613 (1988).
8. J. Newman and W. Tiedemann, *J. Electrochemical Soc.*, **144**, 3081 (1997).
9. D. M. Bernardi, R. Y. Ying, and P. Watson, *J. Electrochem. Soc.*, **151**, A85 (2004).
10. B. Monahov, *ECS Transactions*, **41**, 45 (2012).
11. A. Jaiswal and S. C. Chalasani, *J. Energy Storage*, **1**, 15 (2015).
12. M. Saravanan, M. Ganesan, and S. Ambalavanan, *J. Electrochem. Soc.*, **159**, A452 (2012).
13. A. Banerjee, B. Ziv, E. Levi, Y. Shilina, S. Luski, and D. Aurbach, *J. Electrochem. Soc.*, **163**, A1518 (2016).
14. P. T. Moseley, D. A. J. Rand, A. Davidson, and B. Monahov, *J. Energy Storage*, **19**, 272 (2018).
15. W. B. Gu, G. Q. Wang, and C. Y. Wang, *J. Power Sou.*, **108**, 174-184 (2002).
16. M. Cugnet, S. Laruelle, S. Grugeon, B. Sahut, J. Sabatier, J. Tarascon, and A. Oustaloup, *J. Electrochem. Soc.*, **156**, A974 (2009).
17. H. Gu, T. V. Nguyen, and R. E. White, *J. Electrochem. Soc.*, **134**, 2953 (1987).
18. D. M. Bernardi and M. K. Carpenter, *J. Electrochemical Soc.*, **142**, 2631 (1995).
19. W. B. Gu, C. Y. Wang, and B. Y. Liaw, *J. Electrochem. Soc.*, **144**, 2053 (1997).
20. V. Srinivasan, G. Q. Wang, and C. Y. Wang, *J. Electrochem. Soc.*, **150**, A316 (2003).
21. H. Metzendorf, *J. Power Sources*, **7**, 281 (1982).
22. K. S. Gandhi, *J. Power Sources*, **277**, 124 (2015).
23. K. S. Gandhi, *J. Electrochem. Soc.*, **162**, A1506 (2015).
24. M. Cugnet, M. Dubarry, and B. Y. Liaw, *ECS Transactions*, **25**, 223 (2010).
25. J. O'M. Bockris and S. Srinivasan, *Electrochem. Acta*, **9**, 31 (1964).
26. P. Ekdunge, K. V. Rybalka, and D. Simonsson, *Electrochem. Acta*, **32**, 659 (1987).
27. J. Newman and W. Tiedemann, *Am. Inst. Chem. Engrs Journal*, **21**, 25 (1975).
28. V. Boovaragavan, R. N. Methakar, V. Ramadesigan, and V. R. Subramanian, *J. Electrochemical Soc.*, **156**, A854 (2009).
29. U. S. Kim, C. B. Shin, S. M. Chung, S. T. Kim, and B. W. Cho, *J. Power Sources*, **190**, 184 (2009).